Review of Experimental Verification Methods of Gyrotron Quasi-optical Mode Converters

Grzegorz Jaworski, Andrzej Francik, Maciej Nowak, and Kacper Nowak

Wrocław University of Science and Technology, Wrocław, Poland

Abstract—This survey presents a review of experimental methods relied upon while implementing gyrotron higher mode generation techniques and performing near electromagnetic field measurements in launcher and quasi-optical mode converters. In particular, the paper focuses on low power (cold) testing of gyrotron quasi-optical mode converters outside of the gyrotron, without the presence of high electromagnetic power and electron beams.

Keywords—gyrotron, high order modes, measurement for quasi-optical systems.

1. Introduction

A gyrotron is a high-power microwave source of coherent electromagnetic radiation, with its frequency within the gigahertz to terahertz range, and with the pulse power level of 50 to 500 kW. The device has a broad range of potential applications, as it may be used, for instance, in nuclear magnetic resonance, plasma diagnostics, spectroscopy, weather monitoring, material processing, high-resolution radar, etc. The operating principle of a gyrotron is based on the electron cyclotron resonance phenomenon [1]–[3]. Gyrotrons use the interaction between an annular electron beam and azimuthal electric field of a circular waveguide mode. Electrons that have a cyclotron frequency set slightly below the resonant frequency of the microwave excited in the cavity, electromagnetic wave takes place. The high-order

Fig. 1. Operating principle of a typical quasi-optical mode converter.

mode EM wave generated within the resonant cavity is converted to a wave beam by the mode converter, is then shaped by mirrors and sent towards the output through a window (Fig. 1).

In order to design quasi-optical mode converters (QoMC), dimensions and the geometry of the mode converter, launcher and mirror system need to be determined. The commonly used analytical equations or graphic methods, such as geometrical optics, allow to obtain preliminary results with a good level of accuracy [4], [5]. These approximate usually serve as a good starting point for further full-wave EM field detailed analysis, performed based on computer simulations. A vector diffraction theory is often applied to simulate converter operation and to predict output beam characteristics. The final stage of the design process consists in experimental verification of the theoretical models. Those examples that are most representative for this specific area of research have been selected and are described in this paper.

2. General Remarks on Measurement Setup

Converter design-related mistakes and implementation phase errors need to be eliminated in order to avoid any further problems. Any errors in the QoMC design should be detected before the device starts to operate at maximum power output. Due to high manufacturing costs and considerable health risks associated with powerful gyrotron emissions and the vacuum environment, the so-called cold test method is the only practical method, as it may be deployed without the presence of high levels of EM power [6]–[8]. This method involves measurements of important parameters at safe, low power EM levels. The measurements allow to detect any mistakes made at the design stage or any faults appearing as a result of converter component manufacturing or assembly processes.

A number of methods have been developed to evaluate the performance of the gyrotron QoMC setup. The higher order modes generator is a key element of any "cold test" measuring system. The whispering gallery field mode created by the mode generator is further transformed into
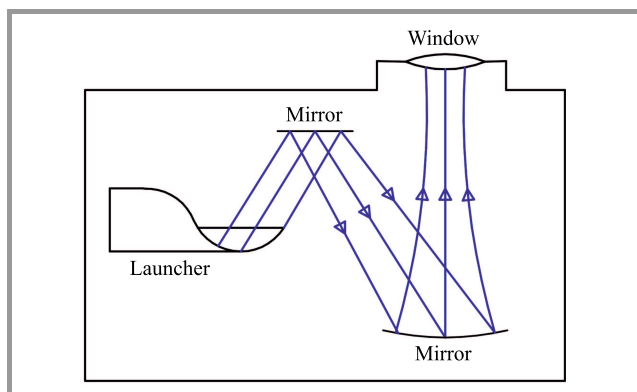
a Gaussian beam using the launcher unit and a mirror system. The standard cold method (from high order mode generator to Gauss beam) requires the design of a higher order mode generator excited by a signal from the vector network analyzer (VNA) instrument, through a set of current sources. In a typical test system, the higher order mode generator is connected between the VNA TX output and the QoMC input tested. The methods of generating rotating and non-rotating modes are further described in Subsection 3.3.

In some types of measurements, the generators may be omitted. It may be assumed that passive quasi-optical systems are reciprocal. This means that lab-class models may be developed based on the method proposed by Vlasov [9]. In this "reversed" design method, the Gaussian beam created in the horn type antenna is further converted into higher order EM modes in the gyrotron resonator, after passing through the mirror system and launcher unit. The next step in such an approach is to design a system that allows to measure these higher order modes. This solution often relies on two identical converter paths connected with each other in both directions (back-to-back) [10]. Such a system is convenient for transmittance measurements. In this setup, fundamental waveguide modes are available at input and output ports, but the transmittance measured in such a setup is two times lower than that of a single converter. The measurements may be easily performed using the VNA instrument. The mode generator and QoMC components are located very close to each other. To measure the fields radiated by them, the near filed measurements methods, using VNA, may be applied. the process is described in greater detail in Section 5. In order to gain insight into the process of field transformation occurring in the QoMC structure, radiation characteristics of the launcher device and the set of mirrors must be determined. This allows to see how the system is changing the geometry of the radiated wave beam. The most important QoMC parameters that should be measured are the radiation characteristics of the launcher and mirrors set. For this purpose, well-known techniques developed for the purpose of antenna near fields measurements are used.

3. Generators of Higher Order Modes

The higher order mode generator is often described in the literature as a converter. This is because of the operating principle, pursuant to which fundamental mode is converted in the waveguide in to a higher order axial mode. The following basic parameters determining the quality of the converter may be distinguished. The first one is conversion efficiency, understood as the ratio between the power of the desired output wave and the power of the input wave, with a gyrotron type of field. Purity is the second important parameter, as it determines the percentage of components related to unwanted field types, in the output spectrum. Bandwidth and physical length of the conversion system are its remaining characteristics. The mode generator allows to create appropriate, higher order azimuthal EM field types, precisely corresponding to those appearing in the gyrotron resonator. Two types of generators are used here. The rotating mode generator (RMG) in which a higher order rotating mode is created is the first of those types. This is a complicated device with low conversion efficiency, but high mode purity. The second type has the form of a non-rotating mode generator (NRMG) [11] in which a non-rotating, higher order mode is created first. This mode is further converted into a rotating mode of the same order using the so-called polarization converter (polarizer). Generators of this type are usually used to generate extremely high order modes (such as $TE_{22,6}$ etc.) [12]. Such devices have a simple design resulting in high immunity to mechanical interference from vibration. Their significant drawback consists in the extremely long waveguide length and, consequently, narrow bandwidth.

Currently, several known methods of generating higher order modes exist:

- converters based on the principle of periodically disturbance of the geometry of the waveguide wall, which gradually transforms the basic type into a higher order waveguide [12]–[14],

- converters inducing the higher order bay mode through the perforated side wall of the bay (translucent cavity wall), using a fader in the form of a quasi-optical mirror [15],

- converters using Y type power dividers to generate relatively low order modes, such as $TE_{0,1}$, $TE_{2,1}$, $TE_{4,1}$ [16]. Units of type offer high conversion efficiency, high signal purity and high bandwidth. Due to their symmetrical coupling structure, they may only generate fields that have even azimuth indices of low order fields, such as circular type $TE_{2,1}$ or $TE_{4,1}$.

3.1. Excitation of Selected Higher Order Modes

Excitation of the selected mode may be achieved by using properly spaced electric or magnetic current sources. The current sources may be created by excitation probes or loops, as well as by coupling apertures in waveguide wall. The electromagnetic field inside a circular waveguide is excited by all induced magnetic moments P_m. The method of exciting modes from any electric or magnetic source is described in [17]. In a typical solution presented in [18], [19], rectangular waveguide sections with the fundamental $TE_{1,0}$ mode are connected to a circular waveguide via coupling apertures on the waveguide's side wall. To excite a pure TE_{m1} mode, magnetic current sources must be applied. For example, to excite $TE_{2,1}$ and $TE_{4,1}$ modes, two and four coupling apertures have to be used, respectively. For excitation of the mode which has a circular distribution of the electric field, selective use of two, four or even more magnetic dipoles may be required.

3.2. Excitation of Rotating Higher Order Modes

Non-rotating modes may be converted into rotating modes of the same-order using the so-called polarization con-

verter [20]. The reported conversion efficiency in this method exceeds 63%, with −2 dB within the 92 to 95 GHz range [20]. The EM wave with circular polarization may be decomposed into two waves with linear polarization and equal amplitudes, being shifted in phase by 90°, however. It follows that the TE$_{m,1}$ wave with circular polarization may be generated by the TE$_{m,1}$ wave with linear polarization and its degenerated wave TE$_{m,1}$. The linearly polarized TE$_{m,1}$ wave propagates along a circular waveguide and reaches the polarizer. As a polarization converter, a mode converter with azimuth wave rumbling is used. The polarizer radius is expressed as follows:

$$r(\varphi) = a_0 + a_1 \cos(10\varphi) \ , \tag{1}$$

where a_0 is the average polarizer radius, a_1 is the deformation and $a_0 \gg a_1$. The TE$_{m,1}$ wave with linear polarization is gradually transformed into its degenerate wave TE$_{m,1}$ due to deformation of the waveguide wall. The length of the deformation, the amplitude of the deformation and the length of the transition section are optimized to obtain two output modes of equal amplitude, but with phase shifted by 90°. With higher deformation, the polarizer length will decrease, but the difficulty of manufacturing increases significantly. Two types of rotating mode generators may be distinguished: high-order rotating mode generators with a perforated cavity wall [21], [22] and rotating mode generators with linear mode conversion [23].

3.3. General Remarks on Mode Generator Design

The complexity of design problems increases along with the number of mode orders to be excited. When a selected mode is excited, other types with a lower cut-off frequency can also be excited. For example, to excite the TE$_{4,1}$ mode, you must consider the possibility of excitation of as many as 14 undesirable modes. This means that when exciting the TE$_{4,1}$ mode, the concentration of the remaining 14 modes should be kept as low as possible. There are several dozen different undesirable modes within the terahertz frequency range. For practical use, the most suitable ones are those for which a large separation between neighboring modes can
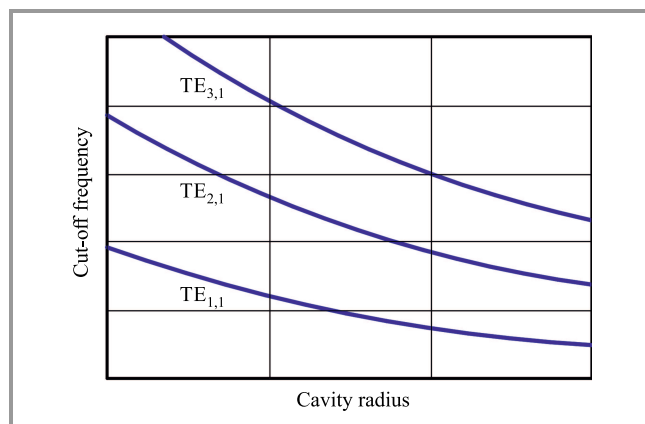

Fig. 2. Circular waveguide cut-off frequency as a function of waveguide radius.

be achieved, thus leading to high modal purity. Conversion losses caused by dissipation of ohmic energy on the copper walls of the converter may be a serious problem as well. However, for higher order mode generators, transmission efficiency is usually less important than modular purity.

The first step in the converter design procedure is to select the circular waveguide diameter. The cut-off frequencies for subsequent modes increase as the waveguide diameter decreases (Fig. 2). To increase separation between successive modes, a coaxial waveguide with a center conductor may be used. The presence of an internal conductor has an effect on the spectrum of the modes' eigenfrequencies. This makes the coaxial waveguides spectrum much more spread compared to circular waveguides.

The suppression of undesirable modes near the working mode can be achieved by selecting the appropriate diameter ratio C:

$$C = \frac{r_{out}}{r_{in}} \ , \tag{2}$$

where r_{out} and r_{in} are the radiuses of the outer conductor and inner coaxial waveguide. More specifically, the coaxial waveguide with a properly selected C ratio should support the propagation of the desired mode and block the propagation of higher order modes.

For a coaxial waveguide with C ratio propagation characteristics for the selected mode, TE$_{m,n}$ may be obtained by solving the following equation [21]:

$$J'_m(\chi_{mn})Y'_m\left(\frac{\chi_{mn}}{C}\right) - J'_m\left(\frac{\chi_{mn}}{C}\right)Y'_m(\chi_{mn}) = 0 \ . \tag{3}$$

When the radius of the outer conductor is much larger than the radius of the center conductor, then:

$$\frac{\chi_{mn}}{C} \to \infty \ , \tag{4}$$

and the equation for the boundary conditions of the coaxial waveguide cross-section is simplified to:

$$J'_m(\chi_{mn}) = 0 \ , \tag{5}$$

which determines the cut-off frequency for a field type in a circular waveguide. In practice, a smooth tapered transition is often used to gradually increase the C ratio for external and internal conductors (Fig. 3). The waveguide and mode converter designed in this way create an open resonance structure that can further improve modal purity of the desired field type.

To avoid the competition effect between modes, a resonator with a high Q factor should be designed. The high value of the resonator additionally allows to reach the operating point with a high coupling efficiency of the beam with an RF field [23]. To handle higher power levels, the size of the transverse cavity must be increased, which simultaneously lowers coupling efficiency of the beam and radiation levels. The cavity quality factor may be expressed as [23]:

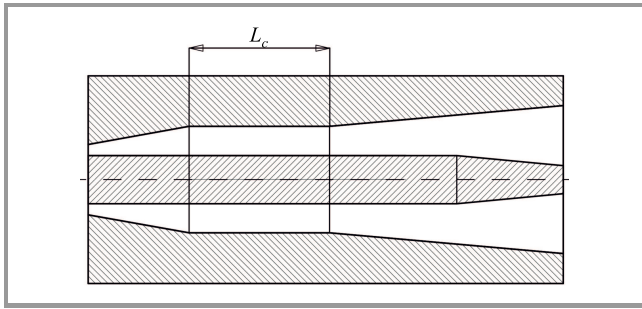$$Q = 4 \cdot \pi \left(\frac{L^2}{\lambda^2}\right) \cdot \left(\frac{1}{1-\rho}\right) \ , \tag{6}$$

Fig. 3. Circular waveguide with tapered transitions and internal conductor.

where L is the effective length of cavity and ρ is the reflection coefficient.

Mechanical design is essential for the mode generator. It is important to maintain both simplicity of the structure and the resulting resistance to mechanical interference and vibrations. An important disadvantage of generators with a complicated mechanical design is the need to perform precise adjustments of the quasi-optical elements before commissioning the devices. At higher frequencies within the terahertz range, the elements have to be fabricated with the level of accuracy down to single micrometers. This technology is currently under development [24].

4. Measurements for Quasi-Optical Systems

Individual components of the QoMC converter are usually positioned close to each other. Therefore, for measuring EM fields, near-field measurement methods have been developed. The term "near-field" is defined as the distance from the antenna, remaining in the range of $\frac{\lambda}{2\pi}$ to $\frac{2D^2}{\lambda}$ [25]. A typical measuring setup used to measure antennas or devices in the near field is shown in Fig. 4.

The system consists of an RF signal source, two frequency mixers with a properly selected local oscillator and a phase/amplitude receiver. All those components constitute a simplified VNA unit [26]). There is also the tested device (DUT) and the measuring probe. Two computer-controlled electro-mechanical positioners are responsible for the appropriate scanning geometry.

The measurements of field distribution in the entire QoMC are reduced to scanning individual elements, assuming that their location in space is appropriate. This means that starting from the first element, e.g. the Vlasov launcher in the gyrotron's internal mode converter, the distribution of radiation at the place of attachment of the second element (quasi-elliptical cylinder mirror) is checked first, and then the field reflected from the second element is measured at the location of the third element (mirror phase correction), and so on. Based on such a procedure, the entire quasi-optical system may be characterized, making it much easier to detect possible errors and allowing to quickly introduce some adjustments to the design at the cold testing

stage. It should be noted that adding another component of the QoMC requires that the scanner's orientation be adjusted relative to the tested system. The direction of the scan axis, which serves as a reference point for starting the scanning procedure, must coincide with the direction of radiation from the tested components, maintaining the radial representation of geometrical optics [27], [28]. Scanning systems comprising different quasi-optic elements (QoE) use different scanning geometries, and implementation of the right geometry may be difficult and complicated.
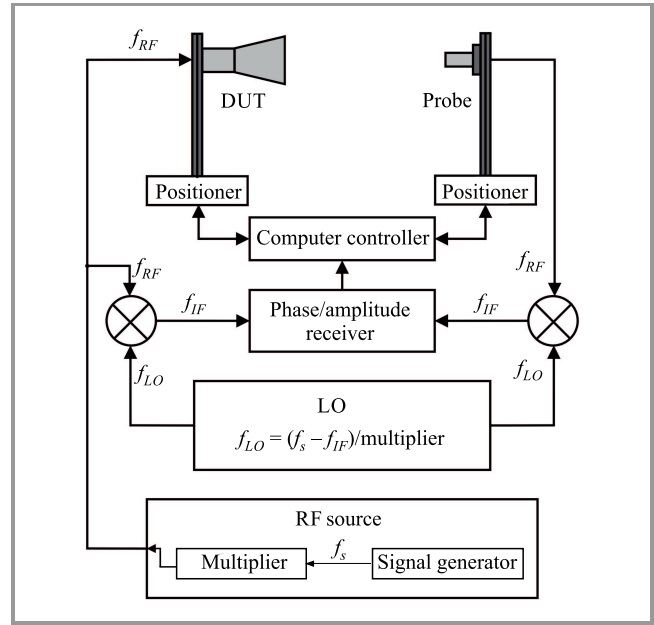

Fig. 4. Block diagram of the measuring system used to measure antennas/devices in the near field.

In classic field scanners, there are three basic scanning geometries – planar, spherical and cylindrical, for which different solutions are provided [25], [29], [30]. A robotic arm may be used for the above cases and for unusual surface mapping with the right number of degrees of freedom [31], [32]. For example, helical (in a cylindrical coordinate system) or spiral (in Cartesian and spherical coordinate systems) scanning techniques significantly reduce the scanning time of antennas in the near field [33]. This is important when we want to quickly perform a near-to-far field transformation, but appropriate non-redundant transformations based on the interpolation method should be used [33]–[41]. In the case of a quasi-optical mode converter, the far field may be taken into account when considering radiation outside the gyrotron window. Regardless of the scanning method used in the measurement of near-field, many factors need to be taken into consideration, including [29]: absorber and its placement, cross-talk and leakage, cable flexing, noise and dynamic range, nonlinearity, normalization, scan area truncation, sampling criteria, separation distance between the test antenna and the probe, probe selection and correction.

Most near-field scanning systems are capable of accurately measuring amplitude, while measuring the phase of radi-

ation patterns at millimeter-wave frequencies still remains a challenging problem [42]. In the millimeter and submillimeter wave ranges, the conventional heterodyne receiver is not immune to phase errors introduced by wiring and by environmental conditions. Generally, amplitude and phase correction [43], [44] should be applied, for example by using multiple receivers [45]–[47] or by applying a phase recovery algorithm from planar scanner maps at different distances from the DUT [48], [49]. This is important in the case of high order rotating gyrotron modes, where phase information is necessary for a good analysis of the quasi-optics mode converter.

4.1. Planar Scanning

As the name implies, a planar scanner (Fig. 5) senses radiation on a plane rather than a rotating surface, which greatly simplifies its design. In addition, most of the beam fields are limited to halfspace [50], and its efficiency in data collection and processing [51] makes it suitable for the work of many research groups [30], [52]–[55]. QoE is most often stationary here, while the probe (scanning antenna) is moved along the x-y plane. The movement is performed line-by-line, the results of the experiment are taken in the region where the disappearing waves (non-propagative types of field) are not important and the probe position increments less than $\lambda/2$ in both x and y directions [29]. This is necessary in order to meet the Nyquist sampling criterion and to avoid aliasing. Due to the limited measuring surface, planar scanning is suitable for measurements at the output taper of mode generator (before entering the launcher). Each scanning point P is represented with the use of Cartesian coordinates x, y, z, where $z = d = $ constans.
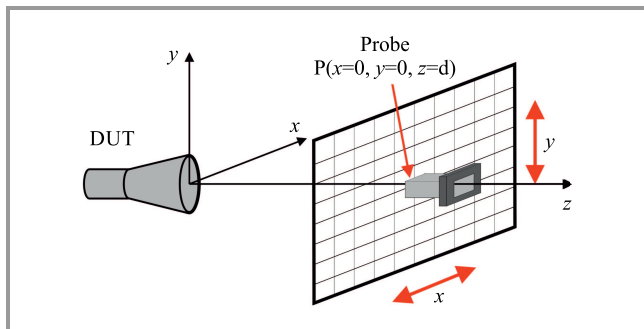

Fig. 5. Near-field planar x-y scanner.

In publication [56], a four-axis configuration of a planar scanner (x, y, z, rotation) is used, with the device also being capable of serving as a spherical scanner, but for a far-field distribution. The planar scanner was used to measure field distribution from the gyrotron output, after attenuation of the signal, with a 2 Hz repetition rate, 140 GHz, mode $TE_{0,1}$. The radiation pattern was measured from the "snake" to verify the conversion of the $TE_{0,1}$ mode to $TE_{1,1}$.

Many other researchers also use the type of scanning geometry described in [30], where the scanner design allows

to measure quasi-optical elements in the frequency range of 110–220 GHz [30], [57], [58]. In paper [52], researchers used a planar scanner for mirror design for high-power gyrotrons. Field intensity measurements of the third mirror and exit window were also carried out by authors in [44]. Other scientists using EO probes also performed measurements of field distribution in the near-field, at an extremely small distance from the converter aperture, on its outer and inner sides, and measurements of the total mode transformation inside the mode converter. The position of the EO probe is controlled by a programmable table, enabling it to be slid along the x-y-z axes [45], [46]. Planar geometry is also used for scanning the beam at the output of the pre-bunching converter [28]. Planar scanners are also used to measure field distribution of quasi-optical generators [22].

4.2. Cylindrical Scanning

Usually, the scanner uses a positioner that rotates QoE along the angular coordinate φ and has a linear scanner (motor) moving the probe along the y axis (Fig. 6).
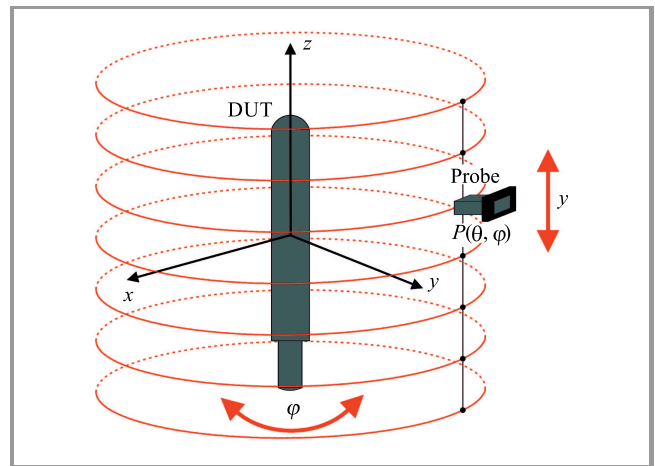

Fig. 6. Cylindrical scanner concept – DUT/QoE rotator for azimuth rotation and probe of the linear y scanner.

The combination of QoE azimuth rotation and a linear probe is equivalent to scanning on a cylindrical surface around QoE. In practice, two measurement scenarios are considered. The first is requires smooth QoE rotation and change of the probe position. The other is requires a smooth probe sweep along the y axis and angular QoE rotation. The cylindrical scanning method is particularly useful for testing fan-beam antennas that have a wide beam in one plane, but a narrow beam in the orthogonal plane [29]. Detailed considerations for this type of scan may be found in papers [29], [33], [59]. The author of [27], [60], measured the filed radiation pattern from the Vlasov launcher at the first mirror location. The study was performed at power level in the range of megawatts, 3 μs pulsed gyrotron operating in the $TE_{22,6}$ mode at 146 GHz. A very similar scan was performed by the scientist in [61]. The measurements were made for a megawatt gyrotron operating at 148.8 GHz in the $TE_{16,2}$ mode.

In all methods, EM field is scanned utilizing a two- or three-axial linear movement unit. Either the probe or QoE are installed on the linear actuator, allowing pixel-by-pixel scanning. In some cases, there is a need to perform image post-processing in order to take into account probe characteristics, scanning curvature or other influences.

4.3. Spherical Scanning

As far as antenna technologies are concerned, the spherical scanning method is widely described in [29], [33], [62], [63] and is used quite often, too. The working principle of the scanner is shown in Fig. 7.
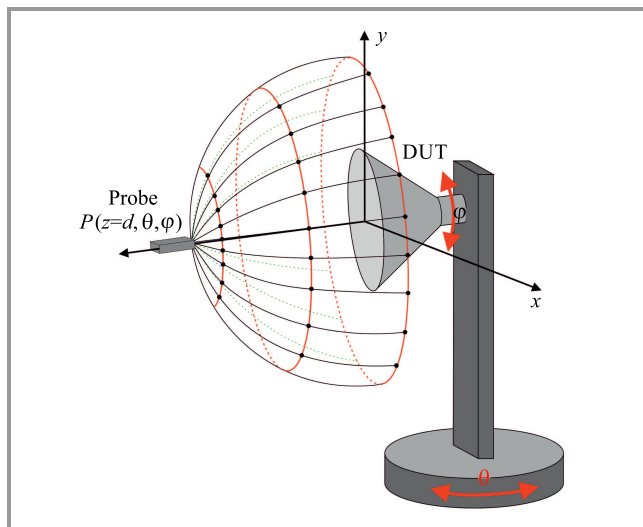

Fig. 7. Spherical scanner: principle of operation.

In the literature concerning QoMC, no examples were found to indicate its use for near-field measurements. Therefore, this type of scanning is performed at the output of the QoMC, at a limited angle of 6 and at a distance exceeding near-field limitations [50]. An example is the snake QoMC carried out in the range of $\theta \pm 30°$ (sphere segment). The scanner was deployed by placing the Labjack on a pivot arm, where the pivot point was below the waveguide output aperture. Spherical scanning in the far-field has also been used and researched in [62] to determine the optimal cutting angle for the Vlasov mod converter. However, we point to the possibility of using spherical geometry, e.g. for scanning the hyperboloid or paraboloid surface that corresponds to the mirror surface. In addition, by using transformation, the spherical surface may be transformed into other analytically defined surfaces.

5. Measurement Probes

The probes are the most important part in the electromagnetic near-field measurement setup. Selection of the appropriate probe type and its dimensions determines which component of the EM field may be measured and with what spatial resolution [64].

The most common types of probes include miniature horn antennas, open-ended waveguides [65] and coaxial probes with one or two (differential probes) coaxial cables [64]. Open-ended probes are used to measure the electrical component, while closed loop probes are used for the magnetic component [66]. Solutions are also in place using electro-optical effects, allowing for very accurate measurement of EM field distributions.

For example, in [64], the use of an optical probe allowed the authors to reduce spatial resolution 5 times compared to monopole coaxial probes (from 500 to 100 μm). These types of probes are especially suitable for performing measuring in microelectronics [67]–[69] and for measuring the phase of QoE. No other types of probes provide such good results that would be as close to the results of numerical simulations relying on full-wave description [70].

The use of EO probes to identify whispering gyrotron gallery mode patterns [55] is the best example here. This paper compares $TE_{6,2}$ mode generator measurements obtained using the VNA scan system employing the WR08 open-ended waveguide probe, using EO probes and micro-EO probes, with the results of CST Microwave Studio simulation data. The results show significant limitations of near-field measurements performed with the use of open-ended probe systems. Despite good SNR levels, resolution and accuracy of the measurements are worse and depend on the size of the probe itself and on its large metal surface exposed. Micro-EO probes provided accurate magnitude and phase measurements identifying mode rotation data in the near field. The authors indicate that mode purity values of CW and CCW rotation equaled 98.11% and 99.8%, respectively. In addition, electro-optical probes, as the only ones listed here, allow to measure the field inside such structures as mode generators, converters, and resonators [13]. In the case of QoE measurements performed in the gyrotron, the TE field type is most often used. However, it should be borne in mind that designs exist supporting the TM field. This emphasizes the need for EO probes measuring E field and H field components. The E field component may be measured using the electro-optic effect of crystals [71]–[82], the converse piezoelectric effect [83]–[86] or electrostatic attraction [87]–[90]. EO probes measure the H field component based on the Faraday effect [91], [92], magnetostriction [93]–[104] or refractive index tunability of magnetic fluid [105]–[115]. The operating principle of the individual probes was described very well by scientists in [116]. In addition, they showed a table with the parameters of various EO probes, including the detection mechanism, sensor probe configuration, detection range and sensitivity/resolution.

Figure 8 contains a schematic of the electro-optical probe that is most frequently used in QoMC sensors.

The electro-optic probe is the most common solution used in QoMC. It is based on the Pockels effect [58], where refractive index change is caused by the EM field's interaction with the crystal. This change may be observed and measured as variation in polarization. The other approach incorporates a non-metallic material (most often a $LiNbO_3$
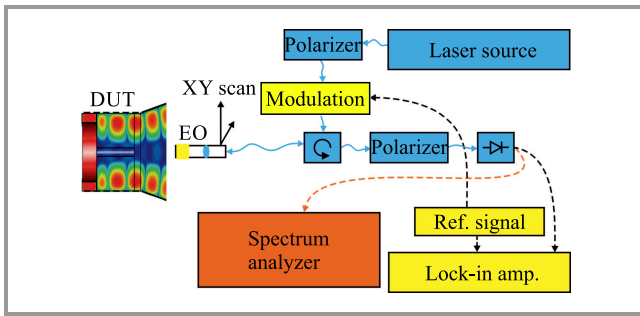
Fig. 8. Diagram describing the electro-optic detection process: lock-in amplifier (purple), spectrum analyzer (purple), and EO – electro-optic crystal (blue lines are fiber connections, dashed lines are copper wires).

crystal [116], [58]) that has very little effect on EM field distribution, but will change its physical properties when EM field is applied, used as a sensing element. The polarized laser beam is used as an information carrier, as it measures the change in physical properties of the sensor material. Either polarization or intensity variations are usually detected while using the optical spectrum analyzer. Additionally, laser light is modulated with a reference signal to achieve better sensitivity and to enable the use of a lock-in amplifier. Light is detected directly or by the Mach-Zehnder interferometer. The test setup may be optically coupled – in this case a fiber circulator is used to separate the signal coming into and leaving the EO probe crystal and a gradient index (GRIN) lens is usually used to couple the laser between the fiber and the EO crystal. Open space configurations are used as well. To provide linear polarization, the polarizer is employed at the laser output. A second polarizer is inserted just before the detector and is used to filter light that has been changed in the EO crystal. In this manner, the detecting sensor will measure different light intensities and the detected change will be proportional to the shift in polarization, based on the Pockels effect caused by the EM field.

Photoconductive antennas (PCAs) may also be used as sensors for terahertz electromagnetic fields. Such an application of those antennas has been described, inter alia, in [117]. There are several other probes for radiation pattern measurements [56], which are placed on a plane that is perpendicular to the radiation source. These include, among others, pyroelectric cameras [118], [119] consisting of an array of pyroelectric elements, thermal paper [120], and liquid crystal sheets [121].

6. Summary

This paper has reviewed the wide scope of the experimental verification methods of the gyrotron quasi-optical mode converters. The only practical option for safe and precise measurements of the QoMC is the so-called "cold test method" without the presence of high EM power and also without the necessity to provide a good quality vacuum. Using such a technique the complete system of the

resonator, taper, launcher and mirrors set can be explored, by using of precise but vulnerable measuring equipment. The key component of the cold test test bed is the higher order modes generator.

The launcher and mirrors set can be considered as a system of radiating components operating at terahertz frequency range. Therefore, for measuring EM field nearby the radiators the methods developed to perform measurements in an antenna near-field can be used. The paper presents numerous examples of such measurement carried out by various teams of researchers. The tests of field distribution in the QoMC are usually reduced to scanning of individual elements with the assumption of their appropriate location in space. The most commonly used systems allow planar and cylindrical scanning. By using transformation, spherical surface can be transformed to other defined surfaces. We believe that this method will allows for scanning the hyperboloid or paraboloid surfaces corresponding to the mirrors surface. The EM field measurements in terahertz frequencies require the use of appropriate transducers that allows to convert the EM field distribution to current or voltage.

Probes are the key element in the EM near field measurement setup. The selection of the appropriate probe type determines the measured component of the EM field and the measurements spatial resolution obtained. The paper describes various types of probes used and their advantages and limitations. A very promising solution is the application of electro-optical effects, allowing for very accurate measurement of EM field distribution. The use of an optical probes allowed to reduce spatial resolution 5 times compared to monopole coaxial probes. Some non-standard methods such as thermal paper, pyroelectric cameras or liquid crystal sheet may also be considered however these methods give usually low quality images.

References

[1] J. W. Gewartowski and H. A. Watson, *Principles of Electron Tubes*. New Jersey: D. Van Nostrand, 1965 (ISBN: 9780442026509).

[2] A. S. Gilmour Jr, *Microwave Tubes*. Boston: Artech House, 1986 (ISBN: 9780890061817).

[3] S. Y. Liao, *Microwave Electron Tubes*. New Jersey: Prentice-Hall, 1988 (ISBN: 9780135820735).

[4] M. K. Alaria and A. K. Sinha, "Design and development of mode converter for 170 GHz gyrotron", *Int. J. of Engin. and Innov. Technol.* (*IJEIT*), vol. 6, no. 6, pp. 17–20, 2016 (DOI: 10.17605/OSF.IO/ERDXK).

[5] J.-W. Liu and Q. Zhao, "Research and design of the quasi-optical mode launcher for the gyrotron", *J. of Infrared and Milim. Waves*, vol. 34, no. 1, pp. 60–65 and 73, 2015 (DOI: 10.3724/SP.J.1010.2015.00060).

[6] V. Yadav *et al.*, "Cold test of cylindrical open resonator for 42 GHz, 200 kW gyrotron", *Sadhana*, vol. 38, no. 6, pp. 1347–1356, 2013 (DOI: 10.1007/s12046-013-0156-y).

[7] P. J. Castro *et al.*, "Cold tests of A 10-GHz gyrotron cavity", *J. of Infrared and Milim. Waves*, vol. 13, no. 1, pp. 91–104, 1992 (DOI: 10.1007/BF01011210).

[8] G. Dammertz, S. Alberti, A. Arnold, E. Giguet, Y. LeGoff, and M. Thumm, "Cold test measurements on components of the 1 MW, 140 GHz, CW gyrotron for the stellarator Wendelstein 7-X", *Fusion Engin. Des.*, vol. 53, no. 1–4, pp. 561–569, 2001 (DOI: 10.1016/S0920-3796(00)00534-2).

[9] S. N. Vlasov and I. M. Orlova, "Quasioptical transformer which transforms the waves in a waveguide having a circular cross section into a highly directional wave beam", *Radiophys. and Quantum Electron.*, vol. 17, no. 1, pp. 115–119, 1974 (DOI: 10.1007/BF01037072).

[10] Z. H. Geng *et al.*, "Simulation and measurement of a W-band circular TE62 mode generator for gyrotrons", in *Proc. 18th Int. Vacuum Electron. Conf. IVEC 2017*, London, UK, 2017 (DOI: 10.1109/IVEC.2017.8289613).

[11] S. G. Kim *et al.*, "Cold testing of quasi-optical mode converters using a generator for non-rotating high-order gyrotron modes", *Rev. of. Sci. Instruments*, vol. 85, no. 10, 2014 (DOI: 10.1063/1.4898180).

[12] N. L. Alexandrov, G. G. Denisov, D. R. Whaley, and M. Q. Tran, "Low power excitation of gyrotron type modes in a cylindrical waveguide using quasi-optical techniques", *Int. J. of Electron.*, vol. 79, no. 2, pp. 215–226, 1995 (DOI: 10.1080/00207219508926263).

[13] I. Lee, D. J. Lee, and E. Choi, "In situ endoscopic observation of higher-order mode conversion in a microwave mode converter based on an electro-optic probe system", *Opt. Express*, vol. 22, no. 22, 2014 (DOI: 10.1364/OE.22.027542).

[14] W. Lawson, M. R. Arjona, B. P. Hogan, and R. L. Ives, "The design of serpentine-mode converters for high-power microwave applications", *IEEE Trans. on Microw. Theory Tech.*, vol. 48, no. 5, pp. 809–814, 2000 (DOI: 10.1109/22.841875).

[15] D. Wagner, M. Thumm, and A. Arnold, "Mode generator for the cold test of step-tunable gyrotrons", in *Proc. 27th Int. Conf. on Infrared and Milim. Waves*, San Diego, CA, USA, 2002 (DOI: 10.1109/ICIMW.2002.1076205).

[16] T. H. Chang, C. H. Li, C. N. Wu, and C. F. Yu, "Exciting circular TE01 modes at low terahertz region", *Appl. Phys. Lett.*, vol. 93, no. 11, 2008 (DOI: 10.1063/1.2987486).

[17] D. M. Pozar, *Microwave Engineering*, 4th ed. Wiley, 2011 (ISBN: 9780470631553).

[18] R. D. Wengenroth, "A mode transducing antenna", *IEEE. Trans. on Microw. Theory and Tech.*, vol. 26, no. 5, pp. 332–334, 1978 (DOI: 10.1109/TMTT.1978.1129382).

[19] T. H. Chang, C. H. Li, C. N. Wu, and C. F. Yu, "Generating pure circular TE$_{mn}$ modes using Y-type power dividers", *IEEE. Trans. on Microw. Theory and Tech.*, vol. 58, no. 6, pp. 1543–5150, 2010 (DOI: 10.1109/TMTT.2010.2048252).

[20] C. Moeller "Mode converters used in the doublet III ECH microwave system", *Int. J. of Electron.*, vol. 53, no. 6, pp. 587–593, 1982 (DOI: 10.1080/00207218208901552).

[21] D. Wagner, M. Blank, T. S. Chu, C. Dubrule, K. Felch, and W. Kasparek, "Design and test od mode generators for high order rotating gyrotron modes", in *Proc. Int. Vacuum Electron. Conf.*, Monterey, CA, USA, 2000 (DOI: 10.1109/OVE:EC.2000.847561).

[22] A. Sawant, M. S. Choe, M. Thumm, and E. Choi, "Orbital angular momentum (OAM) of rotating modes driven by electrons in electron cyclotron masers", *Scient. Rep.*, vol. 7, no. 1, 2017 (DOI: 10.1038/s41598-017-03533-y).

[23] D. Ghosh, N. Medicherla, and R. Seshadri, "Design of TE62 mode generator for W-Band gyrotron", *Asian J. of Converg. in Technol.*, vol. V, no. I, 2019 [Online]. Available: http://www.asianssr.org/index.php/ajct/article/view/719/570

[24] T. H. Chang, T. Idehara, I. Ogawa, L. Agusu, and S. Kobayashi, "Frequency tunable gyrotron using backward-wave components", *J. of Appl. Phys.*, vol. 105, 2009 (DOI: 10.1063/1.3097334).

[25] J. Ala-Laurinaho, "ELEC-E4760 THz techniques", Aalto University Department of Electronics and Nanoengineering, May 15, 2018 [Online]. Available: https://mycourses.aalto.fi/course/info.php?id=24692&lang=en

[26] A. Arinold, O. Braz, O. Schindel, H. R. Kunkel, and M. Thumm, "A mm-wave D-band vector network analyzer of high dynamics", in Proc. 29th Eur. Microwave Conf., Munich, Germany, 1999 (DOI: 10.1109/EUMA.1999.338516).

[27] M. Blank, "High efficiency quasi-optical mode converters for overmoded gyrotrons", Ph.D. thesis, Massachusetts Institute of Technology, 1994 [Online]. Available: https://dspace.mit.edu/handle/1721.1/34089

[28] M. Blank, K. Kreischer, and R. J. Temkin, "Theoretical and experimental investigation of a quasi-optical mode converter for a 110-GHz gyrotron", *IEEE Trans. on Plasma Sci.*, vol. 24, no. 3, pp. 1058–1066, 1996 (DOI: 10.1109/27.533113).

[29] C. A. Balanis, *Modern Antenna Handbook*. Wiley, 2008 (ISBN: 9780470036341).

[30] M. Losert, J. Jin, and T. Rzesnicki, "RF beam parameter measurements of quasi-optical mode converters in the mW range", *IEEE Trans. on Plasma Sci.*, vol. 41, no. 3, pp. 628–632, 2013 (DOI: 10.1109/TPS.2012.2232942).

[31] J. A. Gordon *et al.*, "Millimeter-wave near-field measurements using coordinated robotics", *IEEE Trans. on Ant. Propag.*, vol. 63, no. 12, pp. 5351–5362, 2015 (DOI: 10.1109/TAP.2015.2496110).

[32] R. M. Lebrón *et al.*, "A novel near-field robotic scanner for surface, RF and thermal characterization of millimeter-wave active phased array antenna", in *Proc. IEEE Int. Symp. on Phased Array Syst. and Technol. PAST 2016*, Waltham, MA, USA, 2016 (DOI: 10.1109/ARRAY.2016.7832657).

[33] F. Ferrara, C. Gennarelli, and R. Guerriero, "Near-field antenna measurement techniques", in *Handbook of Antenna Technologies*, Z. N. Chen, D. Liu, H. Nakano, X. Qing, and Th. Zwick, Eds. Springer, 2016, pp. 2107–2163 (DOI: 10.1007/978-981-4560-44-3_117).

[34] R. Yaccarino, L. Williams, and Y. Rahmat-Samii, "Linear spiral sampling for the bipolar planar near-field antenna measurement technique", *IEEE Trans. on Ant. Propag.*, vol. 44, no. 7, pp. 1049–1051, 1996 (DOI: 10.1109/8.504314).

[35] O. Bucci, C. Gennerelli, and C. Savarese, "Nonredundant NF-FF transformation with helicoidal scanning", J. Electromagn. Waves Appl., vol. 15, no. 11, pp. 1507–1519, 2001 (DOI: 10.1163/156939301X00076).

[36] O. Bucci, F. D'Agostino, C. Gennarelli, G. Riccio, and C. Savarese, "Probe compensated far-field reconstruction by near-field planar spiral scanning", *IEE – Proc. Microw., Antennas Propag.*, vol. 149, no. 2, pp. 119–123, 2002 (DOI: 10.1049/ip-map:20020265).

[37] F. D'Agostino *et al.*, "An effective near-field – far-field transformation technique for elongated antennas using a fast helicoidal scan [measurements corner]", *IEEE Ant. and Propag. Mag.*, vol. 51, no. 4, pp. 134–141, 2009 (DOI: 10.1109/MAP.2009.5338700).

[38] R. Cicchetti *et al.*, "Near-field to far-field transformation techniques with spiral scannings: a comprehensive review", *Int. J. of Ant. Propag.*, vol. 2014, ID 143084, 2014 (DOI: 10.1155/2014/143084).

[39] S. Costanzo and G. Di Massa, "Near-field to far-field transformation with planar spiral scanning", *J. of Electromag. Waves and Appl.*, vol. 73, 49–59, 2007 (DOI: 10.2528/PIER07031903).

[40] F. D'Agostino, F. Ferrara, C. Gennarelli, R. Guerriero, M. Migliozzi, and G. Riccio, "A nonredundant near-field to far-field transformation with spherical spiral scanning for nonspherical antennas", *The Open Elec. & Electron. Engin. J.*, vol. 3, no. 1, pp. 1–8, 2009 (DOI: 10.2174/1874129000903010001).

[41] F. D'Agostino, F. Ferrara, C. Gennarelli, R. Guerriero, and M. Migliozzi, "An effective NF-FF transformation technique with planar spiral scanning tailored for quasi-planar antennas", *IEEE Trans. on Ant. Propag.*, vol. 56, no. 9, pp. 2981–2987, 2008 (DOI: 10.1109/TAP.2008.928786).

[42] S. L. Smith *et al.*, "A millimeter-wave antenna amplitude and phase measurement system", *IEEE Trans. on Ant. Propag.*, vol. 60, no. 4, 1744–1757, 2012 (DOI: 10.1109/TAP.2012.2186218).

[43] P. Fuerholz and A. Murk, "Phase-corrected near-field measurements of the TELIS telescope at 637 GHz", *IEEE Trans. on Ant. Propag.*, vol. 57, no. 9, pp. 2518–2525, 2009 (DOI: 10.1109/TAP.2009.2024486).

[44] D. J. van Rensburg and G. Hindman, "Sub-millimeter wave planar near-field antenna testing", in *Proc. 3rd Eur. Conf. on Anten. and Propag. EuCAP 2009*, Berlin, Germany, 2009, pp. 1988–1992, 2009 [Online]. Available: https://ieeexplore.ieee.org/stamp/stamp.jsp?tp=&arnumber=5068007

[45] A. Raisanen, A. Lehto, and J. Tuovinen, "Phase pattern and phase center measurements of antennas at 105–190 GHz with a novel differential phase method", in *Proc. 20th Eur. Microw. Conf.*, Budapest, Hungary, 1990, pp. 347–352 (DOI: 10.1109/EUMA.1990.336067).

[46] J. Tuovinen, A. Lehto, and A. Raisanen, "Phase measurements of millimeter wave antennas at 105–190 GHz with a novel differential phase method", *IEE Proc. H, Microw., Ant. and Propag.*, vol. 138, no. 2, pp.114–120, 1991 (10.1049/ip-h-2.1991.0020).

[47] A. Lehto, J. Tuovinen, O. Boric, and A. Raisanen, "Accurate millimeter wave antenna phase pattern measurements using differential phase method with three power dividers", *IEEE Trans. on Ant. and Propag.*, vol. 40, no. 7, pp. 851–853, 1992 (DOI: 10.1109/8.155754).

[48] T. Isernia, G. Leone, and R. Pierri, "Radiation pattern evaluation from near-field intensities on planes," IEEE Trans. on Ant. and Propag., vol. 44, no. 5, pp. 701–710, 1996 (DOI: 10.1109/8.496257).

[49] A. Capozzoli, C. Curcio, G. D'Elia, and A. Liseno, "Millimeter-wave phaseless antenna characterization", *IEEE Trans. on Ant. and Propag.*, vol. 57, no. 7, pp. 1330–1337, 2008 (DOI: 10.1109/TIM.2008.917186).

[50] S. Liao and R. J. Vernon, "A new fast algorithm for calculating near-field propagation between arbitrary smooth surfaces", in *Proc. Joint 30th Int. Conf. on Infrared and Millim. Waves* and *13th Int. Conf. on Terahertz Electron.*, Williamsburg, VA, USA, 2005, vol. 2, pp. 606–607 (DOI: 10.1109/ICIMW.2005.1572687).

[51] A. Yaghjian, "An overview of near-field antenna measurements", *IEEE Trans. on Ant. and Propag.*, vol. 34, no. 1, 30–45, 1986 (DOI: 10.1109/TAP.1986.1143727).

[52] R. Cao and R. J. Vernon, "Improved performance of three-mirror beam-shaping systems and application to step-tunable converters", in *Proc. Joint 30th Int. Conf. on Infrared and Millim. Waves* and *13th Int. Conf. on Terahertz Electron.*, Williamsburg, VA, USA, 2005, vol. 2, pp. 616–617 (DOI: 10.1109/ICIMW.2005.1572692).

[53] D. R. Denison, T. S. Chu, M. A. Shapiro, and R. J. Temkin, "Gyrotron internal mode converter reflector shaping from measured field intensity", *IEEE Trans. on Plasma Sci.*, 27, no. 2, 512–519, 1999 (DOI: 10.1109/27.772280).

[54] M. S. Choe and E. M. Choi, "Experimental study of TE_{01}-TE_{02} mode converter on 28 GHz", in *Proceedings of the Korean Physical Society* (*Plasma 2013*), poster P2-H006.

[55] I. Lee, A. Sawant, M. S. Choe, D. J. Lee, and E. Choi, "Accurate identification of whispering gallery mode patterns of gyrotron with stabilized electro-optic imaging system", *Physics of Plasmas*, vol. 25, no. 1, ID 013116, 2018 (DOI: 10.1063/1.5017558).

[56] M. K. Hornstein, "A continuous-wave second harmonic gyrotron oscillator at 460 GHz", Ph.D. thesis, Massachusetts Institute of Technology, 2005 [Online]. Available: https://dspace.mit.edu/bitstream/handle/1721.1/33939/67551196-MIT.pdf

[57] I. Russo and W. Menzel, "4–8 GHz near-field probe for scanning of apertures and multimode waveguides", *IEEE Microw. and Wirel. Compon. Lett.*, vol. 21, no. 12, pp. 688–690, 2011 (DOI: 10.1109/LMWC.2011.2173324).

[58] K. Yang, L. P. B. Katehi, and J. F. Whitaker, "Electric field mapping system using an optical-fiber-based electrooptic probe", *IEEE Microw. and Wirel. Compon. Lett.*, vol. 11, no. 4, pp. 164–166, 2001 (DOI: 10.1109/7260.916331).

[59] W. M. Leach and D. Paris, "Probe compensated near-field measurements on a cylinder", *IEEE Trans. on Ant. and Propag.*, vol. 21, no. 4, pp. 435–445, 1973 (DOI: 10.1109/TAP.1973.1140520).

[60] M. Blank, J. A. Casey, K. E. Kreischer, R. J. Temkin, and T. Price, "Experimental study of a high efficiency quasi-optical mode converter for whispering gallery mode gyrotrons", *Int. J. of Electron.*, vol. 72, no. 5–6, pp. 1093–1102, 1992 (DOI: 10.1080/00207219208925635).

[61] A. W. Möbius, J. A. Casey, K. E. Kreischer, A. Li, and R. J. Temkin, "An improved design for quasi-optical mode conversion of whispering gallery mode gyrotron radiation", *Int. J. of Infrared Milim. Waves*, vol. 13, no. 8, pp. 1033–1063, 1992 (DOI: 10.1007/BF01009050).

[62] B. G. Ruth, K. R. Dahlstrom, D. C. Schlesinger, and F. L. Libelo, "Design and low-power testing of a microwave Vlasov mode converter", in *Proc. IEEE MTT-S Int. Microw. Symp. Digest*, Long Beach, CA, USA, 1989, pp. 1277–1280 (DOI: 10.1109/MWSYM.1989.38960).

[63] P. F. Wacker, "Non-planar near-field measurements: Spherical scanning", Final Report, Oct. 1973–Jul. 1974, National Bureau of Standards, Boulder, CO. Electromagnetics Div., 1975 (DOI: 10.6028/nbs.ir.75-809).

[64] Chevallier, D. Baudry, and A. Louis, "Improvement of electrical near-field measurements with an electro-optic test bench", *Progr. in Electromag. Res.*, vol. 40, pp. 381–398, 2012 (DOI: 10.2528/PIERB12020107).

[65] D. Baudry, A. Louis, and B. Mazari, "Characterization of the open-ended coaxial probe used for near-field measurements in EMC applications", *Progr. in Electromag. Res.*, vol. 60, pp. 311–333, 2006 (DOI: 10.2528/PIER05112501).

[66] R. Borisov, K. Zlatkov, and P. Dankov, "Near-field measurements using low cost equipment for RF device characterization", *Electrotech. & Electron.* (*E+E*), vol. 49, no. 3–4, pp. 7–12, 2014 [Online]. Available: https://eplus.tceptt.com/wp-content/uploads/2018/10/20140304-02.pdf

[67] L. Bouchelouk, Z. Riah, D. Baudry, M. Kadi, A. Louis, and B. Mazari, "Characterization of electromagnetic fields close to microwave devices using electric dipole probes", *Int. J. of RF and Microw. Comp.-aided Engin.*, vol. 18, no. 2, pp. 146–156, 2008 (DOI: 10.1002/mmce.20274).

[68] Y. T. Manjombe, Y. Azzouz, D. Baudry, B. Ravelo, and M. E. H. Benbouzid, "Experimental investigation on the power electronic transistor parameters influence to the near-field radiation for the EMC applications", *Progr. in Electromag. Res.*, vol. 21, pp. 189–209, 2011 (DOI: 10.2528/PIERM11092302).

[69] D. Baudry *et al.*, "Near-field probes characterization and inter-laboratory comparisons of measurements", in *Proc. 7th Int. Worksh. on Electromag. Compatib. of Integr. Circ. EMC Compo 2009*, Toulouse, France, 2008.

[70] Y. P. Hong, D. J. Lee, N. W. Kang, and H. Koo, "Phase-stabilized W-band planar imaging system for near-to-far-field projection based on photonic sensors", *IEEE Anten. and Wirel. Propag. Lett.*, vol. 17, no. 2, pp. 315–318, 2018 (DOI: 10.1109/LAWP.2017.2788401).

[71] Z. R. Wang, B. Yu, and W. Z. Chen, "Design and application of an integrated electro-optic sensor for intensive electric field measurement", *IEEE Trans. on Dielec. and Elec. Insul.*, vol. 18, no. 1, pp. 312–319, 2011 (DOI: 10.1109/TDEI.2011.5704523).

[72] Q. Yang, S. Sun, R. Han, W. Sima, and T. Liu, "Intense transient electric field sensor based on the electro-optic effect of $LiNbO_3$", *AIP Adv.*, vol. 5, no. 10, 2015 (DOI: 10.1063/1.4934720).

[73] C. Han, S. Dong, H. Son, and H. Ding, "A novel all-fiber electric field sensor based on tapered fiber-slab waveguide coupler", *Instrum. Sci. & Technol.*, vol. 42, no. 3, pp. 278–289, 2014 (DOI: 10739149.2013.865215).

[74] N. Stan *et al.*, "Optical sensing of electric fields in harsh environments", *J. of Lightw. Technol.*, vol. 35, no. 4, pp. 669–676, 2017 (DOI: 10.1109/JLT.2016.2631149).

[75] H. Togo, N. Kukutsu, N. Shimizu, and T. Nagatsuma, "Sensitivity-stabilized fiber-mounted electrooptic probe for electric field mapping", *J. of Lightw. Technol.*, vol. 26, no. 15, pp. 2700–2705, 2008 (DOI: 10.1109/JLT.2008.927612).

[76] Y. Gaeremynck, G. Gaborit, L. Duvillaret, M. Ruaro, and F. Lecoche, "Two electric-field components measurement using a 2-port pigtailed electro-optic sensor", *Appl. Phys. Lett.*, vol. 99, 2011 (DOI: 10.1063/1.3646103).

[77] S. Mathews, G. Farrell, and Y. Semenova, "All-fiber polarimetric electric field sensing using liquid crystal infiltrated photonic crystal fibers", *Sens. and Actuat. A. Phys.*, vol. 167, no. 1, pp. 54–59, 2011 (DOI: 10.1016/j.sna.2011.01.008).

[78] Y. Zhao, Y. N. Zhang, Q. R. Lv, and J. Li, "Electric field sensor based on photonic crystal cavity with liquid crystal infiltration", *J. of Lightw. Technol.*, vol. 35, no. 16, pp. 3440–3446, 2017 (DOI: 10.1109/JLT.2016.2576500).

[79] T. Zhu, Z. Ou, M. Han, M. Deng, and K. S. Chiang, "Propylene carbonate based compact fiber Mach-Zehnder interferometric electric field sensor", *J. of Lightwave Technol.*, vol. 31, pp. 1566–1572, 2013 (DOI: 10.1109/JLT.2013.2254466).

[80] C. Han, F. Lv, C. Sun, and H. Ding, "Silica microwire-based interferometric electric field sensor", *Opt. Lett.*, vol. 40, pp. 3683–3686, 2015 (10.1364/OL.40.003683).

[81] H. J. Lee, S. J. Kim, M. O. Ko, J. H. Kim, and M. Y. Jeon, "Tunable, multiwavelength-swept fiber laser based on nematic liquid crystal device for fiber-optic electric-field sensor", *Opt. Commun.*, vol. 410, pp. 637–642, 2018 (DOI: 10.1016/j.optcom.2017.11.029).

[82] X. Chen *et al.*, "Liquid crystal-embedded tilted fiber grating electric field intensity sensor", *J. of Lightwave Technol.*, no. 16, vol. 35, pp. 3347–3353, 2017 (DOI: 10.1109/JLT.2016.2643163).

[83] J. Zhao, H. Y. Zhang, Y. S. Wang, and H. W. Liu, "Fiber-optic electric field sensor based on electrostriction effect", *Appl. Mechan. Mater.*, vol. 187, pp. 235–240, 2012 (DOI: 10.4028/www.scientific.net/AMM.187.235).

[84] H. Anirudh, M. V. Reddy, R. L. N. S. Prasad, and B. Sobha, "DC electric field measurement using FBG sensor", in *Proc. of the Worksh. on Recent Adv. in Photon. WRAP 2015*, Bangalore, India, 2015, pp. 1–5, 2015 (DOI: 10.1109/WRAP.2015.7805952).

[85] Q. Liu, Z. Zhang, X. Fan, J. Du, L. Ma, and Z. He, "A novel optical fiber electric field sensor", in *Proc. of the Asia Commun. and Photon. Conf.*, Shanghai, China, 2015 (DOI: 10.1364/ACPC.2014.ATh3A.193).

[86] Y. Yao, B. Yi, J. Xiao, and Z. Li, "FBG based intelligent sensors and structure for electrical power system", in *Proc. of the Int. Conf. on Smart Mater. and Nanotechnol. in Engin.*, Harbin, China, 2007, vol. 6423 (DOI: 10.1117/12.779626).

[87] K. Zhang, H. Zhao, Y. Yang, and W. Zhang, "High voltage electrostatic sensor based on Fabry-Perot interferometer", *Acta Opt. Sinica*, vol. 34, no. 11, 2014 (DOI: 10.3788/AOS201434.1106002).

[88] A. Javernik and D. Donlagic, "Miniature, micro-machined, fiber-optic Fabry-Perot voltage sensor", *Opt. Express*, vol. 27, no. 9, pp. 13280–13291, 2019 (DOI: 10.1364/OE.27.013280).

[89] A. Roncin, C. Shafai, and D. Swatek, "Electric field sensor using electrostatic force deflection of a micro-spring supported membrane", *Sens. and Actuat. A Phys.*, vol. 123–124, pp. 179–184, 2005 (DOI: 10.1016/j.sna.2005.02.018).

[90] A. Kainz *et al.*, "Distortion-free measurement of electric field strength with a MEMS sensor", *Nature Electron.*, vol. 1, pp. 68–73, 2018 (DOI: 10.1038/s41928-017-0009-5).

[91] L. Sun, S. Jiang, and J. R. Marciante, "All-fiber optical magnetic-field sensor based on Faraday rotation in highly terbium-doped fiber", *Opt. Express*, vol. 18, no. 6, pp. 5407–5412, 2010 (DOI: 10.1364/OE.18.005407).

[92] L. Cheng, J. Han, L. Jin, Z. Guo, and B. O. Guan, "Sensitivity enhancement of Faraday effect based heterodyning fiber laser magnetic field sensor by lowering linear birefringence", *Opt. Express*, vol. 21, no. 25, pp. 30156–30162, 2013 (DOI: 10.1364/OE.21.030156).

[93] D. Davino, C. Visone, C. Ambrosino, S. Campopiano, A. Cusano, and A. Cutolo, "Compensation of hysteresis in magnetic field sensors employing Fiber Bragg Grating and magneto-elastic materials", *Sens. and Actuat. A: Phys.*, vol. 147, no. 1, pp. 127–136, 2008 (DOI: 10.1016/j.sna.2008.04.012).

[94] I. M. Nascimento, J. Baptista, P. Jorge, J. Cruz, and M. Andrés, "Passive interferometric interrogation of a magnetic field sensor using an erbium doped fiber optic laser with magnetostrictive transducer", *Sens. and Actuat. A: Phys.*, vol. 235, pp. 227–233, 2015 (DOI: 10.1016/j.sna.2015.10.021).

[95] Z. Shao, X. Qiao, Q. Rong, and A. Sun, "Fiber-optic magnetic field sensor using a phase-shifted fiber Bragg grating assisted by a TbDyFe bar", *Sens. and Actuat. A: Phys.*, vol. 261, pp. 49–55, 2017 (DOI: 10.1016/j.sna.2017.05.001).

[96] M. L. Filograno *et al.*, "Triaxial fiber optic magnetic field sensor for magnetic resonance imaging", *J. of Lightwave Technol.*, vol. 35, no. 18, pp. 3924–3933, 2017 (DOI: 10.1109/JLT.2017.2722545).

[97] H. Liu, S. W. Or, H. Y. Tam, and D. S. W. Or, "Magnetostrictive composite-fiber Bragg grating (MC-FBG) magnetic field sensor", *Sens. and Actuat. A: Phys.*, vol. 173, no. 1, pp. 122–126, 2012 (DOI: 10.1016/j.sna.2011.11.005).

[98] S. M. M. Quintero, A. M. B. Braga, H. I. Weber, A. C. Bruno, and J. F. D. F. Araújo, "A magnetostrictive composite-fiber Bragg grating sensor", *Sensors*, vol. 10, no. 9, pp. 8119–8128, 2010 (DOI: 10.3390/s100908119).

[99] S. M. M. Quintero, C. Martelli, A. M. B. Braga, L. C. G. Valente, and C. C. Kato, "Magnetic field measurements based on terfenol coated photonic crystal fibers", *Sensors*, vol. 11, no. 12, pp. 11103–11111, 2011 (DOI: 10.3390/s111211103).

[100] W. He, L. Cheng, L. Yuan, Y. Liang, L. Jin, and B. O. Guan, "Magnetostrictive composite material-based polarimetric heterodyning fiber-grating laser miniature magnetic field sensor", *Chinese Opt. Lett.*, vol. 13, no. 5, pp. 50602–50605, 2015 (DOI: 10.3788/COL201513.050602).

[101] M. Yang, J. Dai, C. Zhou, and D. Jiang, "Optical fiber magnetic field sensors with TbDyFe magnetostrictive thin films as sensing materials", *Opt. Express*, vol. 17, no. 23, pp. 20777–20782, 2009 (DOI: 10.1364/OE.17.020777).

[102] Q. Li and H. Chen, "Design of fiber magnetic field sensor based on fiber Bragg grating Fabry-Perot cavity ring-down spectroscopy", *Photon. Sens.*, vol. 5, no. 2, pp. 189–192, 2015 (DOI: 10.1007/s13320-015-0231-6).

[103] R. M. Silva *et al.*, "Magnetic field sensor with Terfenol-D thin-film coated FBG", in *Proc. of the 22nd Int. Conf. on Opt. Fiber Sensors OFS-22*, Beijing, China, 2012, vol. 8421 (DOI: 10.1117/12.975169).

[104] G. N. Smith *et al.*, "Femtosecond laser inscribed Bragg sensor in Terfenol-D coated optical fibre with ablated microslot for the detection of static magnetic fields", in *Proc. of the 21st Int. Conf. on Opt. Fiber Sensors OFS-21*, Ottawa, Canada, 2011, vol. 7753 (DOI: 10.1117/12.885122).

[105] J. Dai, M. Yang, X. Li, H. Liu, and X. Tong, "Magnetic field sensor based on magnetic fluid clad etched fiber Bragg grating", *Opt. Fiber Technol.*, vol. 17, no. 3, pp. 210–213, 2011 (DOI: 10.1016/j.yofte.2011.02.004).

[106] N. M. Y. Zhang *et al.*, "Magnetic field sensor based on magnetic-fluid-coated long-period fiber grating", *J. of Optics*, vol. 17, no. 6, 2015 (DOI: 10.1088/2040-8978/17/6/065402).

[107] M. Deng, D. Liu, and D. Li, "Magnetic field sensor based on asymmetric optical fiber taper and magnetic fluid", *Sens. and Actuat. A: Phys.*, vol. 211, pp. 55–59, 2014 (DOI: 10.1016/j.sna.2014.02.014).

[108] L. Luo, M. Lahoubi, S. Pu, J. Tang, and X. Zeng, "Reflective all-fiber magnetic field sensor based on microfiber and magnetic fluid", *Opt. Express*, vol. 23, no. 14, pp. 18133–18142, 2015 (DOI: 10.1364/OE.23.018133).

[109] S. Pu and S. Dong, "Magnetic field sensing based on magnetic-fluid-clad fiber-optic structure with up-tapered joints", *IEEE Photon. J.*, vol. 6, no. 4, pp. 1–6, 2014 (DOI: 10.1109/JPHOT.2014.2332476).

[110] J. Rao, S. Pu, T. Yao, and D. Su, "Ultrasensitive magnetic field sensing based on refractive-index-matched coupling", *Sensors*, vol. 17, no. 7, 2017 (DOI: 10.3390/s17071590).

[111] S. Pu, L. Mao, T. Yao, J. Gu, M. Lahoubi, and X. Zeng, "Microfiber coupling structures for magnetic field sensing with enhanced sensitivity", *IEEE Sens. J.*, vol. 17, no. 18, pp. 5857–5861, 2017 (DOI: 10.1109/JSEN.2017.2734908).

[112] J. Xia, F. Wang, H. Luo, Q. Wang, S. Xiong, and V. M. N. Passaro, "A magnetic field sensor based on a magnetic fluid-filled FP-FBG structure", *Sensors*, vol. 16, no. 5, 2016 (DOI: 10.3390/s16050620).

[113] H. Ji, S. Pu, X. Wang, G. Yu, N. Wang, and H. Wang, "Magnetic field sensing based on capillary filled with magnetic fluids", *Appl. Optics*, vol. 51, no. 27, pp. 6528–6538, 2012 (DOI: 10.1364/AO.51.006528).

[114] H. Wang, S. Pu, N. Wang, S. Dong, and J. Huang, "Magnetic field sensing based on singlemode-multimode-singlemode fiber structures using magnetic fluids as cladding", *Opt. Lett.*, vol. 38, no. 19, pp. 3765–3768, 2013 (DOI: 10.1364/OL.38.003765).

[115] A. Mahmood, V. Kavungal, S. S. Ahmed, G. Farrell, and Y. Semenova, "Magnetic-field sensor based on whispering-gallery modes in a photonic crystal fiber infiltrated with magnetic fluid", *Opt. Lett.*, vol. 40, no. 21, pp. 4983–4986, 2015 (DOI: 10.1364/OL.40.004983).

[116] J. Peng, S. Jia, J. Bian, S. Zhang, J. Liu, and X. Zhou, "Recent progress on electromagnetic field measurement based on optical sensors", *Sensors*, vol. 19, no. 13, 2019 (DOI: 10.3390/s19132860).

[117] D. Saeedkia, "Terahertz photoconductive antennas: Principles and applications", in *Proc. of the 5th Eur. Conf. on Anten. and Propag. EUCAP 2011*, Rome, Italy, 2011, pp. 3326–3328.

[118] E. J. Lerner, "Twenty watts of terahertz", *The Industrial Physicist*, 2003 [Online]. Available: https://www.jlab.org/news/articles/twenty-watts-terahertz-industrial-physicist

[119] V. S. Bajaj *et al.*, "A long-term, stable, CW 250 GHz gyrotron with low second harmonic starting currents", to be submitted, 2005.

[120] J. Jelonnek, "Annual Report 2016", Institute for Pulsed Power and Microwave Technology, KIT Scientific Reports, vol. 7745. KIT Scientific Publishing, Karlsruhe 2018 (DOI: 10.5445/KSP/1000078305).

[121] Y. Carmel *et al.*, "A technique to identify electromagnetic modes in oversize waveguides", *IEEE Trans. on Microw. Theory and Tech.*, vol. 32, no. 11, pp. 1493–1495, 1984 (DOI: 10.1109/TMTT.1984.1132879).

comb generators, mixers, detectors, MICs, microwave instruments and – since recently – gyrotron technology. In 1992 he published a monography title "Instrumental Effects in Homodyne Electron Paramagnetic Resonance Spectrometers" (Ellis Horwood & PWN, Chichester, Warszawa, 1989), earning him a D.Sc. degree. In 2001 he was employed as an Associate Professor at his mother Institute. Currently, his work as a Professor Emeritus focuses on terahertz technology.

https://orcid.org/0000-0001-6414-7106
E-mail: andrzej.francik@pwr.edu.pl
Wrocław University of Science and Technology
Wybrzeże Wyspiańskiego 27
50-370 Wrocław, Poland

Grzegorz Jaworski received his Ph.D. degree from Wrocław University of Science and Technology in 1999. From 2003 to 2004, he was with the Firsted-DTU/EMI Department of Denmark Technical University, working on next generation SAR systems. From 2006 to 2007, he was engaged in developing antennas for the International Space Station's Columbus module. Currently, he is an Assistant Professor at the Electronics and Telecommunication Department, Faculty of Electronics, Wrocław University of Science and Technology. His areas of interest include high frequency techniques and technologies for applications in telecommunication, radars, industry and medicine.

https://orcid.org/0000-0002-9172-7437
E-mail: grzegorz.jaworski@pwr.edu.pl
Wrocław University of Science and Technology
Wybrzeże Wyspiańskiego 27
50-370 Wrocław, Poland

Andrzej R. Francik received his M.Sc. in Electronics from Wrocław University of Technology, Poland, in 1969. He started working as a university lecturer in 1970, and was a researcher at the Institute of Telecommunication and Acoustics. His publications are mainly devoted theoretical and practical problems connected with ESR spectrometry. He earned his Ph.D. degree for analyzing systematic distortions originating from the microwave unit, in 1978. His interests include power combiners,

Maciej Nowak Maciej Nowak received his Ph.D. from Wrocław University of Science and Technology in 2016. He is currently an Assistant Professor at the Telecommunication and Teleinformatics Department, Faculty of Electronics, Wrocław University of Science and Technology. He is a member of the Wrocław Terahertz Center. His research interests include: terahertz spectroscopy, spectral imaging techniques, machine learning.

https://orcid.org/0000-0002-7747-4867
E-mail: maciej.nowak@pwr.edu.pl
Wrocław University of Science and Technology
Wybrzeże Wyspiańskiego 27
50-370 Wrocław, Poland

Kacper Nowak received his Ph.D. from Wrocław University of Science and Technology in 2012. He is currently an Assistant Professor at the Electronics and Telecommunication Department, Faculty of Electronics, Wrocław University of Science and Technology. His research interests include: terahertz spectroscopy, gyrotron technology, industrial automation, networking and programming.

https://orcid.org/0000-0002-5980-8237
E-mail: kacper.nowak@pwr.edu.pl
Wrocław University of Science and Technology
Wybrzeże Wyspiańskiego 27
50-370 Wrocław, Poland